High yield synthesis of single-layer graphene microsheets with dimensional control

Zhongxin Chen[1], Ting Huang[1], Bo Cheng Jin[2], Jiantong Hu[1], Hongbin Lu[1], Steven Nutt[2]

1. State Key Laboratory of Molecular Engineering of Polymers, and Department of Macromolecular Science, Fudan University, 220 Handan Road, Shanghai 200433, China
2. Department of Chemical Engineering and Materials Science, University of Southern California, Los Angeles, CA 90089-0241, United States

Abstract: Future composite applications will require dimensional control of graphene microsheets (GMs) to optimize structure and performance. However, realizing this goal in a high yield, cost-effective manner is presently a major challenge. We here demonstrate a simple approach to prepare single-layer GMs with a yield of >90% by one-step hydrothermal treatment of graphene oxide sheets. The addition of poly(vinyl pyrrolidone) is critical for producing single-layer GMs with specific sheet sizes and does not significantly affect the hydrothermal cutting of GMs. Using hydrothermal treatment under different conditions, the lateral dimensions of the single-layer GMs can be tuned to yield specific surface areas over a range of ~3.5 orders of magnitude, from 30 to 9 $\times 10^{-3}$ μm^2.

1. Introduction

Graphene has potential applications as a filler in polymer composites [1], [2] and [3] due to the large specific surface area and exceptional physicochemical properties [4]. Incorporating graphene microsheets (GMs) into a polymer matrix can produce orders of magnitude enhancements to

mechanical, electrical and thermal properties relative to the pristine matrix, and this approach has enormous potential for myriad industrial applications [5]. However, for this approach to be effective, one must exert dimensional control of the GMs (or diameter-to-thickness aspect ratio for nanoplatelets) [6]. Multiple factors must be considered in this regard. Firstly, small GMs can improve the structural homogeneity within composites. The interfacial structure and dynamics near GMs differ significantly from those far from the interface [7], due to confined interface relaxation [8], [9] and [10] and surface-induced polymer crystallization [11]. Small GMs produce interfacial layers with specific structure and dynamics, leading to more uniform distributions within the composite system, as depicted in Fig. 1. Secondly, achieving a desirable strength/toughness balance of composites requires specific GM sizes to ensure adequate particle mobility to effectively dissipate strain energy [10] and [12]. Furthermore, small GMs can impede crack propagation in composites in much the same way that nanoplatelets function in naturally occurring nacre. In nacre, hierarchically stacked inorganic nanoplatelets impart a superior strength-toughness balance [13] and [14]. Thirdly, sufficiently small GMs reportedly reduce resin viscosity [15] and improve overall processing characteristics without introducing additional free volume or stress concentrations [16]. To realize the full potential of these benefits and optimize the performance of graphene–polymer composites, we must first establish an efficient processing route for synthesis of GMs with controlled sizes [6].
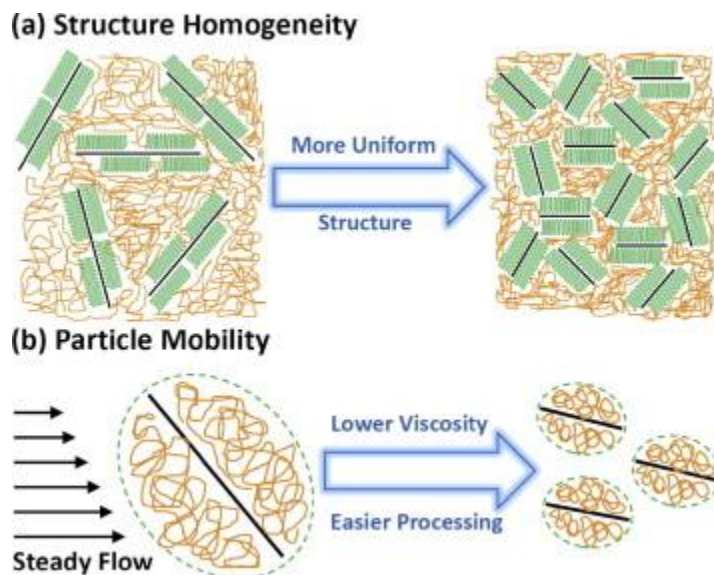
Figure 1: The importance of tuning GM size for optimizing the performance of composites: (a) structure homogeneity and (b) particle mobility. (A colour version of this figure can be viewed online.)

Recent efforts have been dedicated to partitioning large GMs into smaller ones by different methods to meet the requirements of various applications. These processing methods include controlled etching [17], oxidization [18] and [19] and centrifugation [20], particle-assisted nanocutting [21], sonochemistry [22], and hydrothermal cutting [23]. However, despite the partial effectiveness of these techniques, none are suitable for cost-effective production of GMs. Graphene oxide (GO) sheets with controlled dimensions can be prepared by modulating the oxidization time and oxidant content [18]. As described by Menéndez et al., the size of GO sheets can be controlled by adjusting the crystallinity of parent graphite [45], sonication time [46] and the condition employed during hydrazine reduction [47]. Although these methods can be used to control the dimensions of GMs, additional reduction steps are necessary to obtain well-separated GMs. Unlike spherical nanoparticles and nanotubes, plate-like GMs have a strong tendency to form aggregates by interlayer

π–π interaction, especially at high concentrations of GMs. This largely limits their applications in various fields.

In our previous study [23], we demonstrated a hydrothermal approach to simultaneously reduce and tailor GO sheets into smaller GMs. To avoid aggregation during the treatment, a low GO feeding concentration (0.2 mg/mL) was employed. Nevertheless, moderate aggregation of reduced GMs occurred, and thickness increased from 0.7 to 2.2 nm. In principle, it should be possible to prevent the aggregation of GMs by introducing steric hindrance (e.g., polymer) during hydrothermal cutting. However, it remains unclear if adsorbed polymer chain will interfere with the tailoring and reduction of GO sheets, even though it has been observed that the degree of oxidization or the number of defects might affect the hydrothermal cutting of GO sheets [24].

We describe a high-yield (>90%) synthesis method to prepare single-layer GMs with desired lateral dimensions by simple one-step hydrothermal treatment. The addition of a polymer surfactant such as poly(vinyl pyrrolidone) (PVP) preserves the single-layer morphology of the resulting GMs and achieves high yields of the product. This opens a new avenue for the production of GMs for high performance polymer composites.

2. Experimental section

Experimental details can be found in Electronic Supplementary Information (ESI). Briefly, GO was prepared according to Cheng et al. [18] and PVP-GM was prepared using a method modified from previous work [23]. NaOH (100 mg) and PVP (50 mg) were added to 250 ml GO solution (0.2 mg/ml) and sonicated for 10 min to obtain a uniform solution (pH 12). 0.5 ml hydrazine hydrate (50% solution) was then added to the above mixture. Hydrothermal treatment was carried

out in a 500 ml autoclave at 80, 150, and 200 °C for 24 h. No precipitate/aggregate or obvious

change in the pH value of the solution was observed after hydrothermal treatment. The resulting

dark black solution was dialyzed in a dialysis bag (retained molecular weight: 3500 Da) for 5 days

to remove impurities and freeze-dried before use.

3. Results and discussion

3.1 Synthesis of PVP-GMs with dimensional control

GMs (both single and few-layers) with desired lateral dimension and high yield (>90%) were

obtained by simply treating GO with PVP, N_2H_4 and NaOH under hydrothermal conditions (Fig.

S3). Unlike conventional hydrothermal reduction, hydrazine was employed in our hydrothermal

treatment to improve the reduction efficiency of GO sheets [42] and [48]. To verify the cutting

effect in hydrothermal treatment, we examined at least three atomic force micrographs (AFM)

images at a scale of 20×20 or 15×15 μm^2 in tapping mode. Before acquiring AFM micrographs,

all samples were mildly sonicated for 5 min, then spin-coated on the mica surface at 3000 rpm for

30 s.

Representative images of GO and PVP-GMs are shown in Figs. 2 and S7. The lateral dimension of

GO sheets has a wide distribution. The largest GO sheet is ∼50 μm long and ∼35 μm wide and

smaller sheets 1–2 μm wide are also visible. The average surface area of GO is 29.69 μm^2, based

on measurement of at least 100 sheets. Compared to GO, PVP-GMs are much smaller and have a

narrower size distribution. Because of the presence of attached polymers, the thickness of GM is

restricted to single or few layers. With increasing reaction temperature, the lateral dimension of

PVP-GMs decreases from ∼2 μm for PVP-GM-80 °C-24 h to ∼100 nm for PVP-GM-200 °C-24 h. The corresponding average surface areas are 0.822, 0.117 and 9.14×10^{-3} μm^2. This reflects the feasibility of tuning the lateral size of GMs by controlling the reaction temperature. The GM surface area varies by ∼3.5 orders of magnitude as a result of the hydrothermal treatment, and the AFM images provide direct evidence for hydrothermal cutting under these conditions.
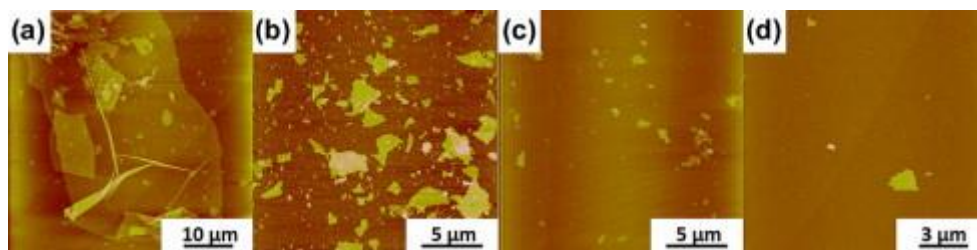
Figure 2: Uniformity of (a) GO, (b) PVP-GM-80 °C-24 h, (c) PVP-GM-150 °C-24 h and (d) PVP-GM-200 °C-24 h by AFM. (A colour version of this figure can be viewed online.)

Given the limited sampling areas of AFM, we also performed field emission scanning electron microscope (FE-SEM), and representative images of GO and PVP-GMs are presented in Fig. 3. Samples were prepared by depositing two drops of the aqueous solutions (0.1 mg/ml) onto a SiO$_2$/Si wafer. Like the AFM observations, the SEM images revealed a wide size distribution of GO sheets, from <10 μm^2 to >1000 μm^2, and most GO sheets had a surface area of ∼100 μm^2, with an average value of 75.0 μm^2. The higher value was attributed to the ultra-large GMs, which were rarely observed in AFM but more frequently seen in FE-SEM. Because of the van der Waals (vdW)/H-bond interaction between GO sheets, some GO sheets overlapped. After hydrothermal treatment (Fig. 3b–d), the lateral dimensions of PVP-GMs gradually decreased with increasing treatment temperature. The average surface areas for PVP-GM-80 °C-24 h, -150 °C-24 h and -200 °C-24 h were 13.3, 7.33 and 2.20 μm^2, respectively. Note that due to electrical charging and the

poor electrical conductivity of the SiO2/Si wafer, PVP-GMs of ~100 nm were difficult to resolve by FE-SEM. Consequently, the dimensions of GO and PVP-GMs observed by FE-SEM were larger than those examined by AFM and transmission electron microscopy (TEM). Nevertheless, the hydrothermal treatment of GO sheets in the presence of PVP resulted in the formation of smaller GMs.
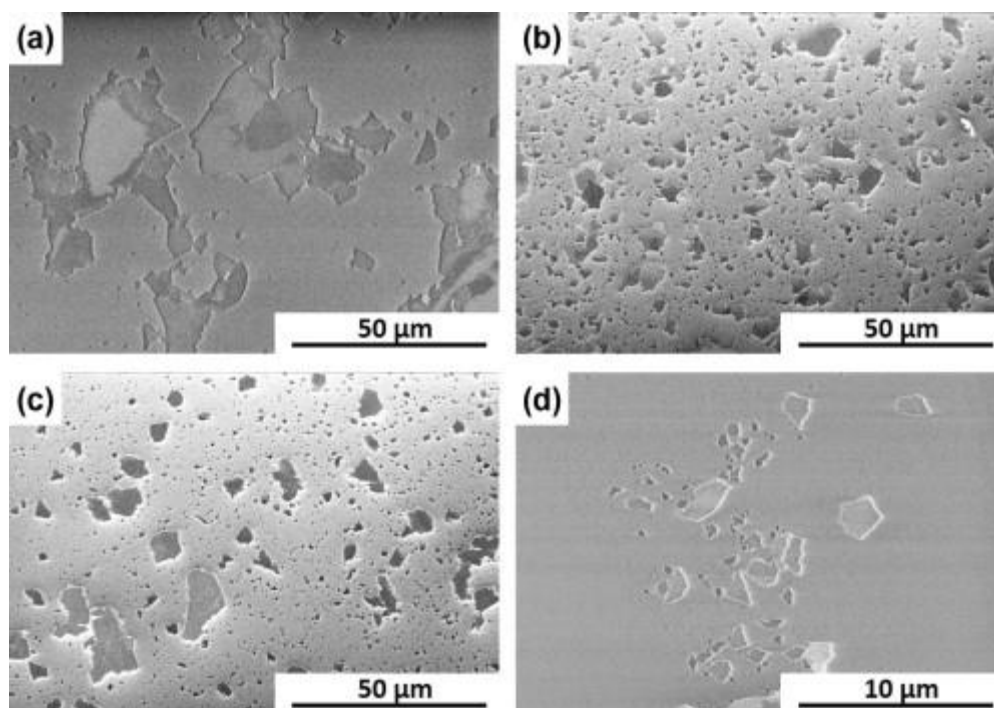
Figure 3: *FE-SEM images of graphene cutting by a PVP-aided hydrothermal process: (a) GO, (b–d) PVP-GM-80 °C-24 h, PVP-GM-150 °C-24 h and PVP-GM-200 °C-24 h.*

The average dimensions of PVP-GMs were calculated from at least 100 microsheets, as shown in Fig. S9 and Table S1. The lateral dimension gradually decreases at higher reaction temperatures or longer reaction times, which translates to an ability to tune the size in a controlled manner. In the next section, we present evidence for the attachment of PVP molecules and their effect on the physico-chemical properties and morphology of PVP-GMs.

3.2 Heading

PVP-GMs produced under different conditions were characterized by thermogravimetric analysis (TGA). As shown in Fig. 4a, GO is thermally unstable and begins to lose weight below 100 °C. The weight loss at 200 °C (21.6%) is less than previously reported (41.7%), suggesting a lower degree of oxidization of GO used in the present study [10] and [23]. PVP is generally thermally stable below 400 °C, but rapidly decomposes at higher temperatures, with a residual weight of ~2.8% at 700 °C. This is consistent with the reported results [25] and [26]. The PVP-GMs exhibit two main weight loss stages in the TGA curves: the first stage spanning 200–400 °C and the second spanning 400–540 °C. The net weight loss of the PVP-GMs is ~53 wt%, part of which can be attributed to the unreduced oxygen functional groups in GMs (4~7 wt%), although the majority comes from the decomposition of PVP (45~48 wt%). The influence of the N-functional groups introduced by hydrazine is considered negligible due to the low content. Additionally, the decreasing weight loss of PVP-GMs with increasing reaction temperatures during the first stage indicates that higher degrees of reduction can be achieved at higher reaction temperatures [27]. The amount of PVP attached to GMs is nearly identical for all PVP-GMs. Given the original feed ratio (1:1 in weight), we conclude that the majority of PVP molecules are attached on GM surfaces during hydrothermal treatment. Furthermore, the attached PVP molecules exhibit a maximum decomposition temperature ~18 °C higher than that of pure PVP, reflecting the fact that GMs effectively suppress the release of volatile components during PVP decomposition.
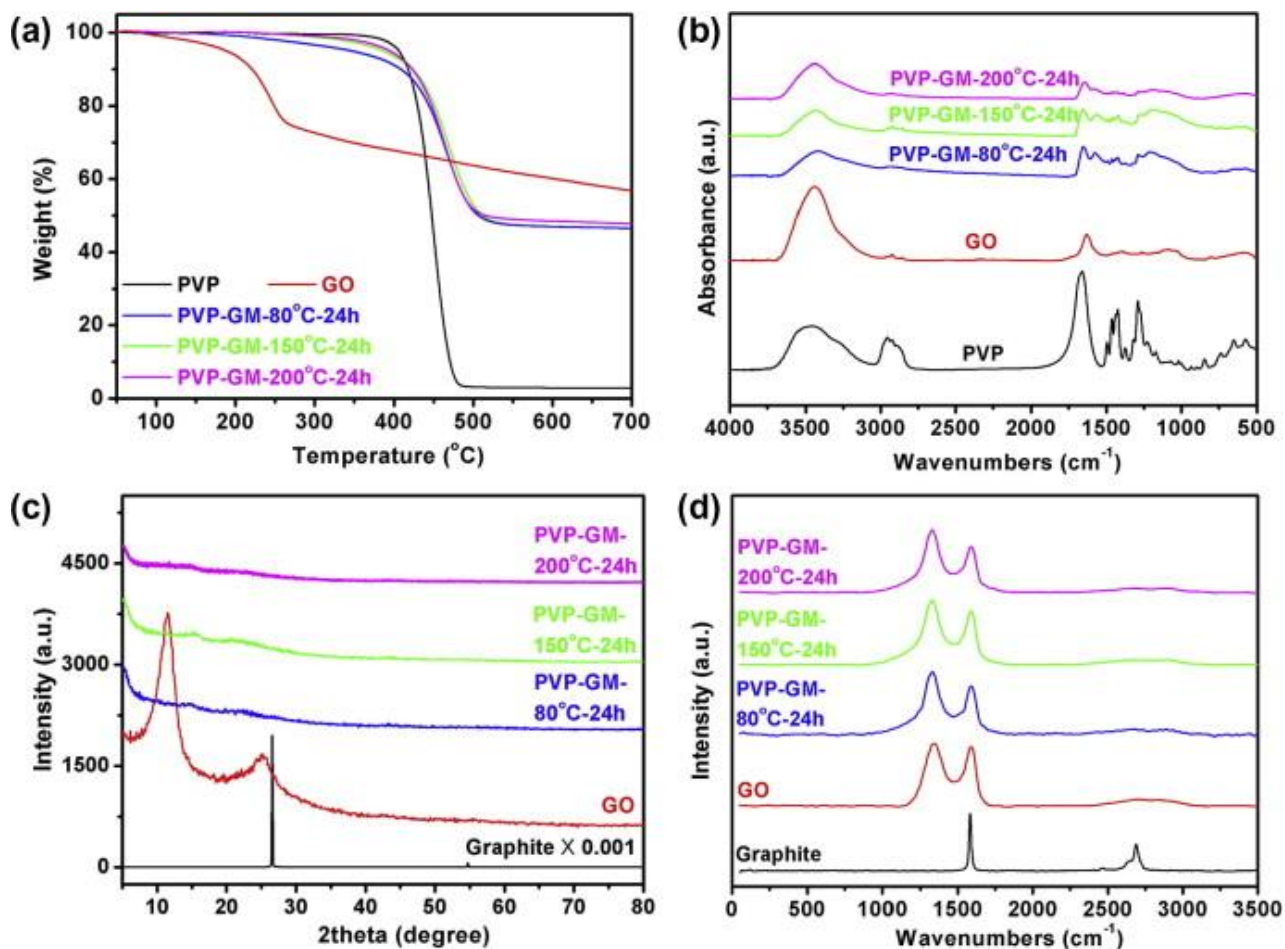
Figure 4: TGA curves (a), FT-IR spectra (b), XRD patterns (c) and (d) Raman spectra of pristine graphite, GO and PVP-GMs obtained at different reaction temperatures. (A colour version of this figure can be viewed online.)

We conducted Fourier transform infrared spectroscopy (FT-IR) experiments to investigate the attachment of PVP molecules and the degree of reduction of PVP-GMs. Multiple bands characteristic of PVP are visible in Fig. 4b: including the alkyl C–H stretching vibrations at 2951, 2922 and 2893 cm−1, the carbonyl groups at 1658 cm−1, the N–H–O complex at 1290 cm−1, and the pyrrolidone ring-related band group at 1461, 1436 and 1423 cm−1[28]. The strong peak of the hydrogen bond arises from residual water in PVP or KBr [29]. After dialyzing for 5 days to remove impurities, all PVP-GMs continue to exhibit the characteristic bands of the N–H–O complex and

pyrrolidone-ring, confirming the existence of PVP molecules on GMs. Also, because of the lower degree of GO oxidation, only two characteristic peaks are observed: one from the free/associated hydroxyl group (∼3440 cm−1), and one from the un-oxidized graphitic domains/adsorbed water molecule (1631 cm−1) [30]. The three weak peaks at ∼1400, 1260 and 1078 cm−1 arise from the vibration of O–H, C–OH and C–O groups on GMs, respectively [31]. These oxygen functional groups are changed after the hydrothermal treatment, and the hydrogen bond peaks significantly decrease for all PVP-GMs. The vibration of sp2 hybridized C bonds shifts to a higher wavenumber (1653 cm−1), indicating that less water is adsorbed in PVP-GMs (increased hydrophobicity). Because the two characteristic bands at 3430 and 1653 cm−1 have comparable intensities, we conclude that similar degrees of reduction of PVP-GMs are achieved at different reaction temperatures.

Structural changes to PVP-GMs are also observed with elemental analysis (EA) and X-ray photoelectron spectra (XPS) (Fig. S10 and Table S2), where compared to other samples, a higher degree of reduction is observed in PVP-GM-200 °C-24 h. With increasing reaction temperature, PVP-GMs exhibit more carbon, but less hydrogen and oxygen in the EA analysis. Similarly, in XPS spectra, the C/O ratios for PVP, PVP-GM-80 °C-24 h, -150 °C-24 h and -200 °C-24 h are 7.64, 8.12, 9.33 and 10.06, respectively. These values are relatively high compared to values for GO (2.26) and reduced-GO (4.72) reported in our previous work [10] and [23], indicating enhanced reduction of GO in the presence of PVP and N2H4. Moreover, the amide groups from PVP, located at 399.7 and 531.2 eV, are the primary species in N1s and O1s core-level spectra. Only a small fraction of amine (400.7 eV) and hydroxyl (533.0 eV) groups are observed. The C1s spectra are fitted with four Gaussian peaks at 284.8, 285.9, 287.6 and 289.0 eV, corresponding to the C–C, C–O/C–N, Cdouble

bond; length as m-dashO and O–Cdouble bond; length as m-dashO species, respectively. The ratio of C–O/C–N to Cdouble bond; length as m-dashO is ~1.95 for all PVP-GMs. Note that amide groups are unlikely be introduced by hydrazine reduction. The N introduced by hydrazine is not taken into account as a result of the limited influence on the C-O/C-N to C = O ratio. Given the theoretical value of PVP (2.00), we assert that the majority of oxygen/nitrogen-functional groups in PVP-GMs result from the attached PVP molecules.

Based on these results, we conclude that increasing hydrothermal reaction temperatures are beneficial for preparing PVP-GMs with higher degrees of reduction. Below, we use X-ray diffraction (XRD) and Raman spectroscopy to further elucidate the possibility that PVP-GMs form aggregates and how the crystalline domain sizes of GMs change during hydrothermal treatment.

Fig. 4c shows XRD patterns of graphite, GO and PVP-GMs. The characteristic diffraction peak at 26.6° arises from pristine graphite. Due to the presence of oxygen functional groups, GO exhibits an expanded interlayer spacing (0.71 nm, relative to 0.33 nm for graphite), corresponding to the strong peak at 11.5°. The relatively weak peak at 25.2° also arises from GO, caused by diffraction from the {0 0 2} of graphite [23]. For all PVP-GMs, however, no characteristic diffraction peaks are seen, indicating the completely exfoliated state of PVP-GMs. This is apparently related to the attached PVP molecules, which cause spatial hindrance and impair π–π interaction between GMs, resulting in relatively loose stacking [8].

Fig. 4d shows Raman spectra for the corresponding samples. Except for graphite, all PVP-GMs exhibit two primary characteristic bands: 1580 cm−1 (graphitic G band) and 1325 cm−1 (defects-induced D band). After hydrothermal treatment at 80, 150 and 200 °C, the D/G intensity ratio

increases from 1.055 (GO) to 1.297, 1.214 and 1.367, respectively. Generally, increased D/G ratios imply more defects in reduced GMs, although intuition suggests that a higher reaction temperature should result in decreased defects. A similar phenomenon was also observed by Ruoff et al., who suggested that the reduction resulted in the formation of new graphitic domains smaller than those present in GO, but greater in number [32]. Another possible explanation is that more sp3 carbon atoms are located at the edges of PVP-GM, implying smaller GMs [33] and [34]. Next, we present evidence for a single-layered morphology of PVP-GMs.

Fig. S8 shows representative AFM images of GO and PVP-GMs samples. GO sheets are smooth, single-layer sheets with a thickness range of 0.70–0.85 nm [10] and [27] with lateral dimensions of 2–3 to tens of microns. After hydrothermal treatment, the lateral dimensions reduce to ~1 μm or less. PVP-GMs manifest rougher surface with visible PVP aggregates, and thicknesses increase to 1.86 nm for PVP-GM-80 °C-24 h. A similar thickness increase is also observed for PVP-GM-200 °C-24 h (2.07 nm), in accord with the previous reports (~2.5 nm [25] and ~2.2 nm [35]). In addition, the PVP aggregates exhibit flat, collapsed pancake morphologies, 10–35 nm in diameter and 0.50–0.65 nm thick. Given that GO is completely reduced and PVP molecules are adsorbed on both sides of GMs, an average thickness for the attached PVP layer is deduced to be of 0.5–0.6 nm. These observations indicate that GMs in the tailored PVP-GMs exist primarily in single-layer form.

The morphologies of GO and PVP-GMs were analyzed by TEM. For clear observation, GO sheets were stained with 1 wt% OsO_4 solution at room temperature for 12 h after depositing on copper grids [36]. GO is transparent and wrinkled, presenting little structural detail at this magnification. Lateral dimensions range from 3 to 15 μm, in accord with the AFM results. The holes and black

aggregates appearing in the image probably arise from the copper grids and are not considered further.

For the PVP-GM-200 °C-24 h shown in Fig. 5b, black, pancake-like aggregates of PVP molecules 20–30 nm in diameter are observed. The distribution of PVP on the surface of GM is not uniform, and the molecules are preferentially situated on the flat basal planes of GMs (rather than at edges). The distribution is attributed to the alkaline hydrothermal environment (pH ∼12) employed during cutting, which forces PVP chains into collapsed configurations on the surface [28]. Such a collapsed configuration is important for cutting large GMs into smaller GMs by the attack of NaOH at reactive sites in GMs. Larger PVP-GMs observed in TEM are attributed to the holy carbon support films used (pore size: 1–2 μm in diameter) and the loss of small GMs during sample preparation. Nevertheless, the TEM images provide direct evidence for hydrothermal cutting of GMs in the presence of PVP.
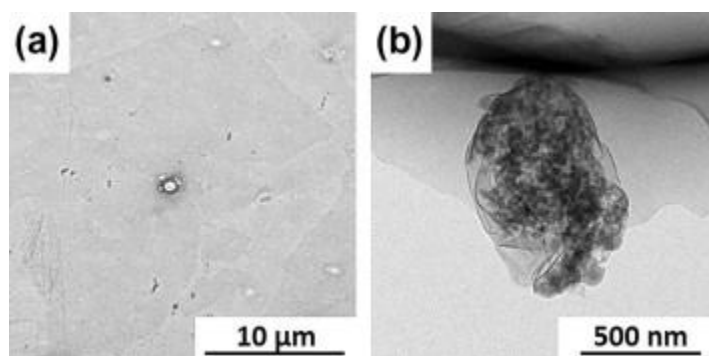
Figure 5: TEM images of (a) GO, stained with OsO₄ and (b) PVP-GM-200 °C-24 h.

3.3 Proposed mechanism for graphene cutting

The cutting or breakage of GMs is closely related to the chemical structure. Unlike the perfect graphene, GO is highly defective and contains oxygen-functional groups (e.g., carboxylic groups at edges and hydroxyl and epoxide groups on basal planes) [37]. A recent study [38] confirmed that the extended π–π network breaks into nanoscale graphitic sp2 domains surrounded by disordered, highly oxidized sp3 domains and carbon vacancy defects during the oxidation of graphite. Also, the aligned epoxy groups play an important role in cutting GMs during the oxidation process [29]. Epoxy groups tend to align on a carbon lattice and the cooperative alignment induces rupture of the underlying C–C bonds [30].

Wang et al. [31], Wu et al. [39] and Tetsuka et al. [40] all reported that under hydrothermal conditions, epoxy pairs induce rupture of C–C bonds, resulting in graphene quantum dots (GQDs) with a diameter of ∼3 nm. Furthermore, the epoxy pairs may be converted to more stable carbonyl pairs, resulting in solubility of GQDs [31] and [41]. Similarly, according to Huang et al. [24] steaming GO sheets for several hours at 200 °C can trigger removal of carbon atoms, which is likely to initiate from the more defective sp3 rich domains. This assertion is supported by our previous work [23], where the temperature dependence of the size during hydrothermal cutting was attributed to defects with different stabilities. The pH value of the solution also plays a role. Coronado et al. reported that reduction under more basic conditions reduces the tendency of aggregation, resulting in fewer defects and larger graphitic domains [42]. The local stress can cause rupture of GM. For example, cutting can be initiated by a point contact between the preoxidized sheet and the AFM probe. Further rupture proceeds linearly along the epoxide groups, yielding microsized graphene

[43]. Under hydrothermal harsh environments, large GMs experience torsional strain and finally break into smaller sheets.

In the present study, GO is rapidly reduced by hydrazine resulting in a variety of N-functional groups (e.g., pyridinic N, pyrrolic N and graphitic N), all introduced from hydrazine [47], [48] and [49]. Higher temperature enables incorporation of more pyridine N into the carbon network of GMs [48]. Meanwhile, the epoxide groups located at GM edges also prefer to form the intermediate hydrazino alcohol, since the latter is thermodynamically more stable than the de-epoxidation products [47]. However, as evidenced by the N1s core-level spectra in Fig. S10c, these N-functional groups are not the main species, a distinction assigned to the amide groups from PVP molecules. Because there is no additional N source available (e.g., ammonia), the content of N-functional groups is low (~1% or less).

To investigate the mechanism of hydrothermal cutting and the time dependence of the size, PVP-GMs were collected in the initial stage of hydrothermal reaction (t = 1, 3, 6 h). The degree of reduction and the lateral dimensions of PVP-GMs were measured, and results are shown in Fig. S11. Briefly, TGA results for PVP-GM-150 °C indicate that reduction of GO is nearly completed in the first 1–3 h. Thereafter, further reduction of PVP-GMs is negligible. This contention is supported by variations in the corresponding Zeta-potential. As shown in Fig. S11c, the Zeta-potential of PVP-GMs rapidly increases from −60 to ~−30 mV in the first 1~3 h, then reaches a stable value (~−33 mV), even when the reaction time is extended to 48 h. Breakage of epoxy pairs is not the main reason for GMs cutting after 3 h. Note that the removal of oxygen functional groups does not directly decrease that of GMs. In fact, the lateral dimension of PVP-GM-80 °C-1 h remains nearly unchanged compared to the size of GO (as shown in Fig. S11d). This assertion is supported by Huang et al.,

who reported that no apparent size reduction was observed after 10 h of steaming [24]. The elimination of oxygen-functional groups may provide a platform for further cutting. For example, consider the dependence of lateral dimensions of PVP-GMs on reaction time, which is calculated and presented in Fig. S9. As shown, higher temperature or longer reaction times result in smaller GM flakes, and the lateral dimensions gradually decrease with time. Note that sonication is not the main reason for graphene cutting, since the size of GO decreases slightly after 30 min sonication, and further decreases can be achieved by prolonging reaction time (Fig. S6a).

Based on the observations presented above, we hypothesize that hydrothermal cutting of GMs occurs in three stages (see Fig. 6): (1) the attachment of PVP molecules on GO surfaces by hydrophobic or electrostatic interaction; (2) rapid reduction of GO by hydrazine; and (3) further reduction. In the second stage, the removal of oxygen functional groups, especially for the epoxy pairs, results in sp3 defect domains in the central plane. These domains are relatively weak and are reactive with the H_2O molecules, etc. Dangling bonds, nanoholes and cracks are created during this process, which initiates the cutting of GMs [24]. Simultaneously, the interaction between GMs is weakened due to the presence of PVP, and consequently no aggregates are formed during reduction. In the third stage, further reduction and local strain partition GMs into smaller sheets. Considering the coverage of PVP and the difference in reactivity between sp3 defect and graphitic domains, water or other reagents are likely to preferentially attack sp3 carbon atoms exposed at GM edges or at defect domains within GMs. In addition, higher temperature will activate defects with lower reactivity, leading to faster cutting and smaller GMs. Given the ID/IG ratio of GO (1.055), the average size of graphitic sp2 domain is determined to be ~32 nm according to the Tuinstra–Koenig relationship [34]. This is much less than the size of PVP-GMs we obtained. Thus, extending the reaction time to

48 h or longer should yield smaller GMs, although it may be impossible to obtain GQDs with mildly oxidized GO.

Figure 5: TEM images of (a)

Another critical factor is the local strain. An epoxy line defect weakens the fracture stress of the sheet by ~16% [44]. Cracks and nanoholes created from the elimination of epoxy pairs will also decrease the mechanical strength of nearby domains, while large GMs are twisted or torqued. Harsh environments also increase the probability for GM fracture due to the high energy input and associated molecular motions. Nevertheless, with the protection of PVP molecules, a lower and more controllable reaction rate can be achieved, and PVP-GMs with specific lateral dimensions and degree of reduction can be prepared at gram-scale levels with yields of >90%.

4. Conclusion

Because the properties of GMs are closely related to their lateral dimensions, it is important for practical applications to be able to prepare GMs with a high degree of dimensional control. In the present study, we demonstrate that PVP-aided hydrothermal treatment can be used to simultaneously reduce and cut GO into single-layer GMs with specific sizes (ranging nearly ~3.5 orders-of-magnitude) by controlling the reaction temperature. As-prepared PVP-GMs were homogenously

dispersed in aqueous solution for one month. The GMs were produced by a simple reaction that offers both high yields (>90%) and cost-effective. Because of this, the process may be suitable for a variety of industrial operations and applications.

The basic mechanism involved in the cutting process was elucidated by investigating the time-dependence of the reaction. We propose that hydrothermal cutting is initiated from the epoxy pairs in the central plane, and further advanced by reaction between H_2O molecules and reactive sp3 carbon atoms, and/or by the strain induced from twisting of GMs.

5. Appendix A. Supplementary data

Supplementary data associated with this article can be found, in the online version, at http://dx.doi.org/10.1016/j.carbon.2013.10.076

References:

Z. Chen, T. Huang, B.C. Jin, J. Hu, H. Lu, and S. Nutt. "High-yield synthesis of single-layer graphene microsheets with dimensional control" Carbon 68 (2013) 167-174 DOI<http://dx.doi.org/10.1016/j.compstruct.2013.09.017>

1. Stankovich S, Dikin DA, Dommett GHB, Kohlhaas KM, Zimney EJ, Stach EA, et al. Graphene-based composite materials. Nature 2006;442:282–6.
2. Ramanathan T, Abdala AA, Stankovich S, Dikin DA, Herrera- Alonso M, Piner RD, et al. Functionalized graphene sheets for polymer nanocomposites. Nat Nanotechnol 2008;3:327–31.
3. Potts JR, Dreyer DR, Bielawski CW, Ruoff RS. Graphene-based polymer nanocomposites. Polymer 2011;52:5–25.
4. Park S, Ruoff RS. Chemical methods for the production of graphenes. Nat Nanotechnol 2009;4:217–24.
5. Ghaffarzadeh K, Thiele C. Graphene opportunities 2013–2018: technology, markets, players, IDTechEX. <http:// www.idtechex.com/research/reports/grapheneopportunities- 2013-2018-technology-markets-players- 000333.asp>.
6. Pan SY, Aksay IA. Factors controlling the size of graphene oxide sheets produced via the graphite oxide route. ACS Nano 2011;5:4073–83.
7. Terrones M, Martin O, Gonza´ lez M, Pozuelo J, Serrano B, Cabanelas JC. Interphases in graphene polymer-based nanocomposites: achievements and challenges. Adv Mater 2011;23:5302–10.
8. Fang M, Wang KG, Lu HB, Yang YL, Nutt S. Single-layer graphene nanosheets with controlled grafting of polymer chains. J Mater Chem 2010;20:1982–92.
9. Fang M, Zhang Z, Li JF, Zhang HD, Lu HB, Yang YL. Constructing hierarchically structured interphases for strong and tough epoxy nanocomposites by amine-rich graphene surfaces. J Mater Chem 2010;20:9635–43.
10. Chen ZX, Lu HB. Constructing sacrificial bonds and hidden lengths for ductile graphene/polyurethane elastomers with improved strength and toughness. J Mater Chem 2012;22:12479–90.
11. Ning NY, Fu SR, Zhang W, Chen F, Wang K, Deng H, et al. Realizing the enhancement of interfacial interaction in semicrystalline polymer/filler composites via interfacial crystallization. Prog Polym Sci 2012;37:1425–55.
12. Munch E, Launey ME, Alsem DH, Saiz E, Tomsia AP, Ritchie RO. Tough, bio-inspired hybrid materials. Science 2008;322:1516–20.
13. Tang ZY, Kotov NA, Magonov S, Ozturk B. Nanostructured artificial nacre. Nat Mater 2003;2:413–8.
14. Espinosa HD, Rim JE, Barthelat F, Buehler MJ. Merger of structure and materials in nacre and bone – perspectives on de novo biomimetic materials. Prog Mater Sci 2009;54:1059–100.
15. Guimont A, Beyou E, Martin G, Sonntag P, Cassagnau P. Viscoelasticity of graphite oxide-based suspensions in PDMS. Macromolecules 2011;44:3893–900.
16. An L, Pan YZ, Shen XW, Lu HB, Yang YL. Rod-like attapulgite/ polyimide nanocomposites with simultaneously improved strength, toughness, thermal stability and related mechanisms. J Mater Chem 2008;18:4928–41.
17. Ci LJ, Xu ZP,Wang LL, GaoW, Ding F, Kelly KF, et al. Controlled nanocutting of graphene. Nano Res 2008;1:116–22.
18. Zhao JP, Pei SF, Ren WC, Gao LB, Cheng HM. Efficient preparation of large-area graphene oxide sheets for transparent conductive film. ACS Nano 2010;4:5245–52.

19. Zhang L, Liang JJ, Huang Y, Ma YF, Wang Y, Chen YS. Size-controlled synthesis of graphene oxide sheets on a large scale using chemical exfoliation. Carbon 2009;47:3365–8.
20. Khan U, O'Neill A, Porwal H, May P, Nawaz K, Coleman JN. Size selection of dispersed, exfoliated graphene flakes by controlled centrifugation. Carbon 2012;50:470–5.
21. Kosynkin DV, Higginbotham AL, Sinitskii A, Lomeda JR, Dimiev A, Price BK, et al. Longitudinal unzipping of carbon nanotubes to form graphene nanoribbons. Nature 2009;458:872–6.
22. Wu ZS, Ren WC, Gao LB, Liu BL, Zhao JP, Cheng HM. Efficient synthesis of graphene nanoribbons sonochemically cut from graphene sheets. Nano Res 2010;3:16–22.
23. Ma C, Chen ZX, Fang M, Lu HB. Controlled synthesis of graphene sheets with tunable sizes by hydrothermal cutting. J Nanopart Res 2012;14:996. 1-9.
24. Han TH, Huang YK, Tan ATL, David VP, Huang J. Steam etched porous graphene oxide network for chemical sensing. J Am Chem Soc 2011;133:15264–7.
25. Zhang JL, Shen GX, Wang WJ, Zhou XJ, Guo SW. Individual nanocomposite sheets of chemically reduced graphene oxide and poly(N-vinyl pyrrolidone): preparation and humidity sensing characteristic. J Mater Chem 2010;20:10824–8.
26. Yang Y, Ren LL, Zhang C, Huang S, Liu TX. Facile fabrication of functionalized graphene sheets (FGS)/Zno nanocomposites with photocatalytic property. ACS Appl Mater Interfaces 2011;3:2779–85.
27. Zhou XH, Chen ZX, Yan DH, Lu HB. Deposition of Fe–Ni nanoparticles on polyethyleneimine-decorated graphene oxide and application in catalytic dehydrogenation of ammonia borane. J Mater Chem 2012;22:13506–16.
28. Dhumale VA, Gangwar RK, Datar SS, Sharma RB. Reversible aggregation control of polyvinylpyrrolidone capped gold nanoparticles as a function of pH. Mater Express 2012;2:311–8.
29. Li Z, Zhang W, Luo Y, Yang J, Hou JG. How graphene is cut upon oxidation? J Am Chem Soc 2009;131:6320–1.
30. Li JL, Kudin KN, McAllister MJ, Prud'homme RK, Aksay IA, Car R. Oxygen-driven unzipping of graphitic materials. Phys Rev Lett 2006;96(1-4):176101.
31. Chen S, Liu JW, Chen ML, Chen XW, Wang JH. Unusual emission transformation of graphene quantum dots induced by self-assembled aggregation. Chem Commun 2012;48:7637–9.
32. Stankovich S, Dikin DA, Piner RD, Kohlhass KA, Kleinhammes A, Jia YY, et al. Synthesis of graphene-based nanosheets via chemical reduction of exfoliation graphite oxide. Carbon 2007;45:1558–65.
33. Lin XY, Shen X, Zheng QB, Yousefi N, Ye L, Mai YW, et al. Fabrication of highly-aligned, conductive, and strong graphene papers using ultralarge graphene oxide sheets. ACS Nano 2012;6:10708–19.
34. Pimenta MA, Dresselhaus G, Dresselhaus MS, Cancado LG, Jorio A, Saito R. Studying disorder in graphite-based systems by Raman spectroscopy. Phys Chem Chem Phys 2007;9:1276–90.
35. Yoon S, In I. Role of poly(N-vinyl-2-pyrrolidone) as stabilizer for dispersion of graphene via hydrophobic interaction. J Mater Sci 2011;46:1316–21.

36. Wei M, Lee J, Kang B, Mead J. Preparation of core-sheath nanofibers from conducting polymer blends. Macromol Rapid Commun 2005;26:1127–32.
37. Kim J, Cote LJ, Huang J. Two dimensional soft materials: new faces of graphene oxide. Acc Chem Res 2012;45:1356–64.
38. Erickson K, Erni R, Lee Z, Alem N, Gannett W, Zettl A. Determination of the local chemical structure of graphene oxide and reduced graphene oxide. Adv Mater 2010;40:4467–72.
39. Pan DY, Guo L, Zhang JC, Xi C, Xue Q, Huang H, et al. Cutting sp2 clusters in graphene sheets into colloidal graphene quantum dots with strong green fluorescence. J Mater Chem 2012;22:3314–8.
40. Tetsuka H, Asahi R, Nagoya A, Okamoto K, Tajima I, Ohta R, et al. Optically tunable amino-functionalized graphene quantum dots. Adv Mater 2012;24:5333–8.
41. Pan DY, Zhang JC, Li Z, Wu MH. Hydrothermal route for cutting graphene sheets into blue-luminescent graphene quantum dots. Adv Mater 2010;40:734–8.
42. Bosch-Navarro C, Coronado E, Martı´-Gastaldo C, Sa´nchez- Royo JF, Go`mez MG. Influence of the pH on the synthesis of reduced graphene oxide under hydrothermal conditions. Nanoscale 2012;4:3977–82.
43. Fujii S, Enoki T. Cutting of oxidized graphene into nanosized pieces. J Am Chem Soc 2010;132:10034–41.
44. Paci JT, Belytschko T, Schatz GC. Computational studies of the structure, behavior upon heating and mechanical properties of graphite oxide. J Phys Chem C 2007;111:18099–111.
45. Botas C, A´lvarez P, Blanco C, Santamarı´a R, Granda M, et al. The effect of the parent graphite on the structure of graphene oxide. Carbon 2012;50:275–82.
46. Botas C, Pe´rez-Mas AM, A´lvarez P, Santamarı´a R, Granda M, Blanco C, et al. Optimization of the size and yield of graphene oxide sheets in the exfoliation step. Carbon 2013;63:576–8.
47. Botas C, A´lvarez P, Blanco C, Gutie´rrez MD, Ares P, et al. Tailored graphene materials by chemical reduction of graphene oxides of different atomic structure. RSC Adv 2012;2:9643–50.
48. Long D, Li W, Ling L, Miyawaki J, Mochida I, Yoon SH. Preparation of nitrogen-doped graphene sheets by a combined chemical and hydrothermal reduction of graphene oxide. Langmuir 2010;26:16096–102.
49. Gao X, Jang J, Nagase S. Hydrazine and thermal reduction of graphene oxide: reaction mechanisms, product structures, and reaction design. J Phys Chem C 2010;114:832–42